



OPEN Comparison of a new type of Dark Matter with the Milky Way and M31 grand rotation curves

Bruce M. Law

In the electron Born self-energy (eBse) model, free electrons are of finite-size and possess both a rest mass, m_e , as well as, a Born mass, $m_e^B = 74,000 m_e$. The Born mass, which originates from the energy contained within the electric field that surrounds a finite-sized electron, serves as a Dark Matter (DM) particle in this theory (designated eBDM, electron Born Dark Matter). The equation of state for m_e^B is $w = -1$, which implies that two Born masses experience a *repulsive* gravitational interaction. This repulsive gravitational interaction stabilizes the formation of a DM halo of m_e^B particles, of typical halo size ~ 100 kpc, around a central mass M (e.g. a galaxy), where this gravitational stability arises from the competing attractive $M - m_e^B$ and repulsive $m_e^B - m_e^B$ interactions. A solution of the linearized Poisson-Boltzmann equation, for this system, allows one to derive an expression for the rotational velocity $V_{eBDM}(R)$, as a function of radius R from the galactic center. A composite model composed of rotational velocity contributions from the galactic bulge, galactic disk, as well as, $V_{eBDM}(R)$ is found to provide a good description of the Grand Rotation Curves for the Milky Way and M31 galaxies.

There are numerous astronomical anomalies that indicate that the Universe is full of Dark Matter (DM)^{1,2}. DM is a type of matter that is known to interact gravitationally but does not interact via the electromagnetic force, namely, DM does not emit, absorb, or reflect light. Light does, however, undergo gravitational lensing in the presence of a large DM mass where, for example, DM galactic halos can distort galactic shapes^{3,4}, for weak lensing, or may even create multiple images of the same galaxy^{3,4}, if strong lensing is present. DM halos are also thought to be the cause of anomalously high stellar⁵⁻⁷ velocities around a galactic center, as well as, high galactic cluster velocities observed in the Coma cluster⁸. These high velocities can only be explained via the presence of significant amounts of DM, over and above the visible baryonic matter⁹. Gravitational lensing has also enabled the observation of a physical separation between the DM and luminous baryonic component, in the collision of two galaxies, within the Bullet cluster^{10,11}. The astronomical observations for DM, discussed thus far, have been on galactic length scales. DM is also required on cosmological length scales in order to understand the expansion history of the Universe. In the current cosmological paradigm, as encapsulated by the Λ CDM model, the Cosmic Microwave Background (CMB) anisotropy requires a significant DM component; this model indicates that the Universe is composed of approximately $\sim 5\%$ baryons (the ordinary matter), $\sim 25\%$ cold DM (CDM), and $\sim 70\%$ Dark Energy (DE)¹². DE is a type of repulsive gravity that has been acting during the last ~ 7 billion years of the Universe's expansion history and is thought to be caused by Einstein's Cosmological constant (the Λ in the Λ CDM model).

Planets, Black Holes, and other non-luminous massive bodies have been ruled out as providing sufficient gravitational interaction to explain DM. CDM is thought to be a slow moving (non-relativistic) particle that interacts gravitationally. But what is CDM? None of the particles in the Standard Model (SM) of particle physics are capable of explaining CDM. CDM is thought to be a new type of particle that lies outside the SM and, thus, if found, would form an extension to the SM. Certain CDM candidate particles (WIMPs, Weakly Interacting Massive Particles) are thought to interact not only gravitationally but also via a weak interaction. If CDM does indeed interact via a weak interaction then this would allow direct detection e.g. at the LHC or at other specialized DM detectors¹. Thus far there have been no confirmed direct detections of any CDM candidate particles. For any DM candidate, extensive work would be required to prove that this DM particle does indeed exhibit the requisite properties in order to explain all of the DM observations listed above.

An alternative approach to explaining the DM observations is to assume that Newtonian gravity is modified at very low accelerations (of order $\sim 10^{-10} m/s^2$)^{13,14}. Such an assumption is able to explain many features attributed to DM, however, MOND (Modified Newtonian Dynamics) is an empirical observation in need of

Department of Physics, Kansas State University, 116 Cardwell Hall, Manhattan, KS 66506-2601, USA. email: bmlaw@phys.ksu.edu

an explanation. Namely, what physical phenomenon gives rise to a modification of Newtonian gravity and, by implication, General Relativity at these low accelerations and why are the modifications of the form assumed in MOND?

Both the Λ CDM model, as well as, MOND exhibit challenges and shortcomings in providing an adequate explanation for the DM astronomical observations. The purpose of this publication is to introduce a new form of DM, arising from the electron Born self-energy (eBse) model, describe its properties, and compare this DM candidate with Grand Rotation Curves (GRC) around the Milky Way and M31 galaxies. GRC data consists of astronomical measurements of the rotational velocities of stars, satellite galaxies, and globular clusters, around the galactic center of spiral galaxies.

This publication is set out as follows. Earlier publications, by the author, considered the cosmological consequences of the eBse model with regards to DE^{15,16} and Cosmic Inflation (CI)¹⁷. The work on DE is of direct relevance to the current discussions and, therefore, is briefly summarized in the Section “[Brief review of the eBse model](#)”. The Section “[Electrostatics near a charged sphere](#)” recalls the well-known electrostatics of a neutral plasma, surrounding a central charge Q , where the physics involved has similarities to our DM discussions. The eBse Dark Matter model is described in Section “[eBse Dark Matter model](#)” where this model is extended to predict the velocity of stars and satellite galaxies around the galactic center as a function of radial distance R . The Section “[Milky Way and M31 GRC analysis](#)” applies the eBse DM model to an analysis of the GRC data for both the Milky Way and M31 galaxies. Finally the Section “[Summary and discussion](#)” provides a summary and discussion of our results.

Brief review of the eBse model

For a flat, homogeneous, and isotropic Universe, General Relativity reduces to the much simpler Friedmann velocity equation given by¹⁸

$$H^2 = \left(\frac{\dot{a}}{a}\right)^2 = \frac{8\pi G}{3c^2} \Pi_{tot} \quad (1)$$

This equation describes the cosmological expansion of the Universe where H is Hubble’s parameter, a is the scale factor, \dot{a} is the scale factor velocity, Π_{tot} is the total energy density of intergalactic space, G is Newton’s gravitational constant, and c is the speed of light in a vacuum. In the Λ CDM model¹⁸

$$\Pi_{tot} = \frac{\Pi^R}{a^4} + \frac{\Pi^B + \Pi^{DM}}{a^3} + \frac{\Pi^{DE}}{a^{3(1+w)}}, \quad (2)$$

which has energy density contributions from radiation (superscript R), baryons (B), DM, and DE. The equation of state for DE has been measured to be^{19,20}

$$w = \frac{p}{\Pi^{DE}} \approx -1, \quad (3)$$

to a good approximation, where p is the pressure. Equation (3) implies that Π^{DE} is a form of “repulsive gravity”, that causes the Universe to accelerate when Π^{DE} is dominant. In Eq. (2) DM and DE are of unknown origin where Π^{DM} and Π^{DE} are treated as adjustable parameters.

The Universe’s expansion switches from a deceleration (when Π^{DE} is sub-dominant early in the Universe’s expansion history at $a \ll 1$) to an acceleration (when Π^{DE} is dominant at $a \simeq 1$) where this switch over from deceleration to acceleration occurs at a redshift of²¹

$$z_{da} \sim 0.8. \quad (4)$$

The Λ CDM model is the currently accepted cosmological paradigm because this model accounts for the CMB anisotropy $\sim 380,000$ years after the Big Bang (BB), recent DE measurements ~ 14 billion years after the BB, as well as, numerous other astrophysical observations¹⁸. The Λ CDM model is supplemented by a period of exponential acceleration (Cosmic Inflation) that occurs prior to the Λ CDM phase. CI is required in order to explain the homogeneity and flatness of the CMB where thermal fluctuations δT have been measured to be remarkable small ($\delta T/T \sim 10^{-5}$)¹⁸. Unfortunately, in the currently accepted cosmological paradigm of CI and Λ CDM there are many unknowns. What caused CI? What is DE? What is DM?

In the eBse model the electron is assumed to be of finite size, with radius

$$R_e = 1.9 \times 10^{-20} m, \quad (5)$$

where the value in Eq. (5) arises from the best experimental estimate deduced from the contact interaction energy between electrons and positrons measured at the LEP (large electron-positron collider)^{22,23}. A finite, non-zero electron radius implies that the Born self-energy of this electron, corresponding to the energy contained in the electric field that surrounds this particle, is given by^{24,25}

$$U_e^B = \frac{e^2}{8\pi\epsilon_0 R_e}, \quad (6)$$

where e is the fundamental unit of charge and ε_0 is the vacuum permittivity. Gravity couples to all energies. Equation (2) is missing contributions from electric field energies in intergalactic space, thus, in the eBse model, Eq. (2) is replaced by^{15,16}

$$\Pi_{tot} = \frac{\Pi^R}{a^4} + \frac{\Pi^B + \Pi^{DM} + \Pi^{elec}}{a^3}, \quad (7)$$

where Π^{DE} has been omitted from Eq. (7) because Π^{elec} quantitatively accounts for phenomena that previously had been attributed to DE. The dominant contribution to Π^{elec} arises from the electron Born self-energy, primarily because the electron radius is so small. Thus,

$$\Pi^{elec} \simeq N_B \nu_e(t) U_e^B \quad (8)$$

where N_B is the baryon number density in intergalactic space today (at $z = 0$), while $\nu_e(t)$ is the **time dependent** fractional ionization in the WHIM (Warm-Hot-Intergalactic-Medium). In the WHIM atomic hydrogen, in cosmic web voids, are attracted to cosmic filaments where they collisionally ionize into free electrons and protons at temperatures of $10^5 - 10^7 K$ ²⁶. This collisional ionization fraction changes with time t

$$\nu_e(t) \sim t^s \quad (9)$$

as the cosmic web evolves. The exponent s determines whether the expansion of the Universe is accelerating ($s \geq 1$) or decelerating ($s < 1$) in this model. As discussed previously^{15,16}, Eqs. (8) and (9) quantitatively account for many features that are attributed to DE. In particular, in the eBse model, (i) Π^{elec} today (at $a = 1$ and $z = 0$) agrees with the magnitude of DE (namely, $\Pi^{DE} = N_B \nu_e(z = 0) U_e^B$), (ii) the ratio of DE to B today (i.e. Π^{DE} / Π^B) can be quantitatively explained, (iii) the equation of state for eBse is identical to Eq. (3), and (iv) the deceleration-acceleration redshift (Eq. (4)) arises from the switch over from $s < 1$ to $s \geq 1$.

There are additional cosmological consequences if electrons and positrons are of finite size. Due to their finite size there will be a maximum number density of $n_{max} = 1 / (2R_e)^3$, for electrons and positrons, as no more than one electron (or positron) can be packed into a volume $(2R_e)^3$. During the early Universe's evolution, at sufficiently high temperatures ($> 1 MeV$), there is a chemical equilibrium between photons and electron-positron pair creation ($2\gamma \leftrightarrow e^- + e^+$). However, this system falls out of chemical equilibrium above a glass transition temperature $T_G = 1.06 \times 10^{17} K$ because the electron and positron number density is constant at n_{max} for $T \geq T_G$ ¹⁷. A constant number density necessarily also implies that the potential energy density is also constant. In cosmology a constant potential energy density gives rise to exponential acceleration, akin to Cosmic Inflation. Thus, the eBse model possesses elements which replicate the behavior of both DE^{15,16} and CI¹⁷ in a single model.

In the eBse model DE arises from the time dependent creation of free electrons, along with their associated Born self-energy U_e^B (Eq. (6)), from the collisional ionization of atomic hydrogen in the WHIM at temperatures of $10^5 - 10^7 K$. In the WHIM there will be other (residual) free electrons present, specifically, free electrons outside the temperature range $10^5 - 10^7 K$. These residual free electrons will also possess an associated U_e^B where their fractional ionization, represented by ν_{e0} , is expected to be time independent. In the eBse model, it is natural to assume that these residual free electrons give rise to effects that should be associated with DM, namely^{15,16},

$$\Pi^{DM} = N_B \nu_{e0} U_e^B \text{ with } \nu_{e0} = 0.127, \quad (10)$$

where the estimate for ν_{e0} arises from the Planck collaboration estimate for the ratio Π^{DM} / Π^B .

To distinguish this new candidate eBse DM "particle" from other DM candidates (e.g. CDM) we will call it the electron Born DM (eBDM) candidate. The small value for R_e , in Eq. (5), gives rise to a surprisingly large electron Born mass of

$$m_e^B = U_e^B / c^2 \approx 74,000 m_e \approx 40 m_p, \quad (11)$$

where m_e and m_p are, respectively, the electron and proton rest masses. As the equation of state (Eq. (3)) holds for m_e^B , this implies that two m_e^B masses are gravitationally repulsive (whereas a neutral, uncharged mass M and m_e^B will be gravitationally attractive). There will be free electrons (forming a halo) around galaxies. An intuitive picture of the underlying physics that gives rise to galactic DM halos around galaxies, in the eBse model, is that there is a central mass M which is surrounded by a halo of Born masses m_e^B around this central mass. The repulsive $m_e^B - m_e^B$ and attractive $M - m_e^B$ interactions stabilize the DM halo in this model (Fig. 1a). The physics for this situation is directly related to the formation and stability of a plasma "halo" that forms around a central (positive) charge Q (Fig. 1b). In this later case the halo stability arises from the fact that like charges repel, whereas, unlike charges attract.

There are some differences between the physics in Figs. 1a compared with Fig. 1b. In Fig. 1b one has electroneutrality and the number of positive charges (+) is balanced by the number of negative charges (-). By contrast, in Fig. 1a, there is only one type of repulsive mass, m_e^B , as the "counterbalancing" repulsive mass arising from the proton Born mass is much, much smaller ($m_p^B \approx 9 \times 10^{-4} m_p$ using $R_p = 8.5 \times 10^{-16} m^{27}$ in Eq. (6)) and, therefore, can be neglected.

Any model, which is able to explain DM, will necessarily be an extension of the Standard Model of particle physics. A requirement for any extension of the SM is that it not create any conflicts with the SM. The eBse

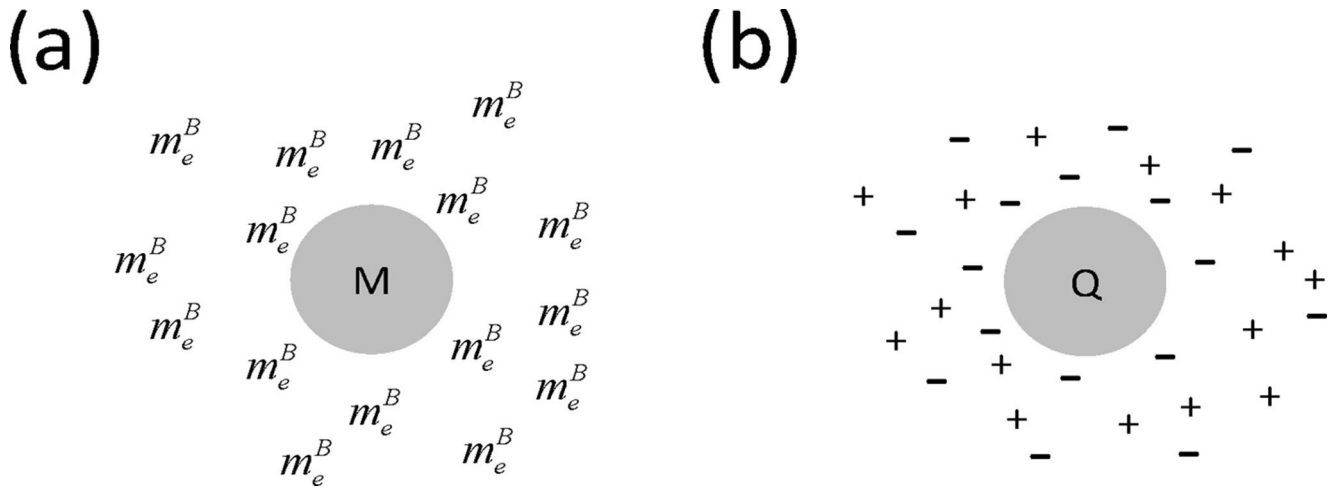


Figure 1. (a) Halo of Born masses around a central mass. (b) Plasma halo of positive and negative charges around a central (positive) charge .

model is an extension of Quantum Electrodynamics (QED); QED forms part of the Standard Model. In QED the electron is assumed to be a point particle ($R_e \rightarrow 0$) and, as a consequence, U_e^B (Eq. (6)) is divergent. This divergence is “renormalized” away, in QED, by assuming that U_e^B is subsumed or contained within m_e . Unfortunately, the elimination of U_e^B in QED implies that (non-local) energy is not conserved when considering the interaction between an electron and a positron¹⁶. Removal of U_e^B also implies that QED is inconsistent with the treatment of ions in Soft Matter physics where the Born self-energy of ions is required to explain the solubility of ions in solution²⁴. In the eBse model the electron is put on an identical footing to other ions, which possess both a normal rest mass, as well as, a Born self-energy while at the same time preserving conservation of energy. As discussed in the [Supplementary Information](#) in¹⁷ the value for R_e , in Eq. (5), is sufficiently small that QED experiments continue to be consistent with QED theoretical predictions, thus, ensuring the integrity of the Standard Model.

Electrostatics near a charged sphere

Before we consider the eBse mass contribution to the Dark Matter galactic halo, it is first useful to review the electrostatics of a plasma of protons and electrons that surround a single fixed test charge Q . Here we follow the presentation of Thorne and Blandford²⁸ Chap. 20. The electrostatic potential $\phi(r)$ outside a charged particle satisfies Poisson’s equation.

$$\begin{aligned} \nabla^2 \phi &= -\frac{\rho}{\epsilon_0} \\ &= -\frac{(n_p - n_e)e}{\epsilon_0} - \frac{Q}{\epsilon_0} \delta(r), \end{aligned} \quad (12)$$

where $\rho = \rho(r)$ is the charge density, $n_i(r)$ is the average number density of protons or electrons ($i = p, e$), while $\delta(r)$ is the Dirac delta function. In the linearized Poisson-Boltzmann approach, where it is assumed that $e\phi \ll k_B T$, then

$$n_p = \bar{n} \exp \left[-\frac{e\phi}{k_B T} \right] \approx \bar{n} \left[1 - \frac{e\phi}{k_B T} \right] \quad (13)$$

$$n_e = \bar{n} \exp \left[+\frac{e\phi}{k_B T} \right] \approx \bar{n} \left[1 + \frac{e\phi}{k_B T} \right] \quad (14)$$

with \bar{n} the mean number density of electrons or protons averaged over a large volume, k_B is Boltzmann’s constant, and T is temperature. In this approximation Eq. (12) reduces to

$$\nabla^2 \phi = \frac{2\phi}{\lambda_D^2} - \frac{Q}{\epsilon_0} \delta(r), \quad (15)$$

where the Debye screening length is given by

$$\lambda_D = \left(\frac{\epsilon_0 k_B T}{\bar{n} e^2} \right)^{1/2}. \quad (16)$$

Equation (15) has solution

$$\phi(r) = \frac{Q}{4\pi\epsilon_0 r} e^{-\sqrt{2}r/\lambda_D}. \quad (17)$$

For later considerations it is useful to consider the Debye screening length λ_D in interstellar and intergalactic media, where the characteristic values are listed in Table 1 below, which were obtained from Table 20.1 in²⁸.

eBse Dark Matter model Galactic halo

According to the previous section the Debye screening length, λ_D , sets the characteristic length scale over which the electron and proton plasma, surrounding a charge Q , decays away. If the analogy in Fig. 1a and b is correct then there should also exist a characteristic gravitational Debye screening length, λ_G , which would set the decay scale for the halo of Born masses, m_e^B , around a central mass M . The interrelationship between λ_D and λ_G is expected to be given by

$$\left(\frac{\lambda_D}{\lambda_G}\right)^2 = \frac{F_G}{F_e}, \quad (18)$$

where

$$F_e = \frac{e^2}{4\pi\epsilon_0 r^2} \quad (19)$$

and

$$F_G = \frac{G(m_e^B)^2}{r^2}. \quad (20)$$

Equations (18)–(20) imply that

$$\lambda_G = 2.8 \times 10^{16} \lambda_D \quad (21)$$

which leads to the values for λ_G given in Table 1. The intergalactic gravitational Debye length

$$\lambda_G^g \approx 91 \text{ kpc} \sim R_h \quad (22)$$

is very similar to typical DM halo radii, R_h . According to Table 1, the interstellar gravitational Debye length

$$\lambda_G^s (\approx 0.009 \text{ kpc}) \ll \lambda_G^g, \quad (23)$$

which will be relevant in later discussions. Equations (16) and (18) imply that

$$\lambda_G = \left(\frac{k_B T}{4\pi\bar{n}G(m_e^B)^2}\right)^{1/2} \quad (24)$$

The magnitudes of λ_D and λ_G , in Table 1, indicate the vastly differing length scales over which electrostatics and “Born mass” gravitational effects are of relevance.

Rotational velocities around a galactic center

The Poisson equation for gravitational fields is given by²⁹

$$\nabla^2\phi = 4\pi G\mu, \quad (25)$$

where μ is the mass density. The *sign* difference between the “electrostatic” Poisson equation (Eq. (12)) and the “gravitational” Poisson equation (Eq. (25)) arises because gravity is always thought of as being attractive. If we consider a central mass M that is surrounded by a gaseous system of atomic hydrogen atoms, of mass m_H , then Eq. (25) becomes

$$\nabla^2\phi = 4\pi G n_H m_H + GM\delta(r), \quad (26)$$

Plasma	$\bar{n} \text{ (m}^{-3}\text{)}$	$T \text{ (K)}$	$\lambda_D \text{ (m)}$	$\lambda_G \text{ (kpc)}^*$
Interstellar medium	10^5	10^4	10	0.009
Intergalactic medium	0.1	10^6	10^5	91

Table 1. Debye screening lengths. *1 kiloparsec (kpc) = 3.086×10^{19} m.

where the number density of hydrogen atoms is described by a Boltzmann distribution

$$n_H = \bar{n}_H \exp \left[-\frac{m_H \phi}{k_B T} \right] \approx \bar{n}_H \left[1 - \frac{m_H \phi}{k_B T} \right] \tag{27}$$

Equations (26) and (27) reduce to

$$\nabla^2 \phi = 4\pi G \bar{n}_H m_H - \frac{\phi}{(\lambda_G^H)^2} + GM\delta(r), \tag{28}$$

where λ_G^H represents the corresponding gravitational Debye length, but for atomic hydrogen (Eq. (24) with m_e^B and \bar{n} replaced by m_H and \bar{n}_H , respectively). Upon comparison of Eq. (15) with Eq. (28), the key difference is the **sign** of the ϕ term on the right hand side. Equation (28) has solution

$$\phi(r) = \frac{k_B T}{m_H} + \frac{GM}{r} e^{-ir/\lambda_G^H} \tag{29}$$

where the $e^{-ir/\lambda_G^H}/r$ term represents a spherical wave, corresponding to gravitational collapse. Namely, as expected, a central mass M surrounded by atomic hydrogen is unstable. In Newtonian gravity, a description of gravitational collapse is obtained by combining Eq. (25) with the continuity and Euler equations, which leads to the gravitational Jeans instability³⁰.

Equation (26) can be generalized to

$$\begin{aligned} \nabla^2 \phi &= 4\pi G [\mu + n_H m_H + n_{He} m_{He} + n_p m_p + n_e (m_e - m_e^B)] + GM\delta(r) \\ &\approx 4\pi G (\mu - n_e m_e^B) + GM\delta(r) \end{aligned} \tag{30}$$

which is more representative of the situation for galactic systems where, in the first line, a central mass M is surrounded by ordinary matter, with mass density $\mu = \mu(r)$, as well as, a gaseous cloud of atomic hydrogen, helium, and ionized hydrogen (free electrons and protons). In this first line the electron Born mass, m_e^B , makes an appearance but with a change in **sign** because, as mentioned before, two m_e^B are repulsive. In the second line, in Eq. (30), only the dominant terms have been retained. In the following we consider a simplified model, with $\mu = 0$, in order to examine how the eBse term influences stellar rotational velocities far from the galactic center (i.e. M represents a galactic mass, $M \sim (10^9 - 10^{13})M_\odot$ where M_\odot is a solar mass).

In Eq. (30) the number density

$$n_e = \bar{n} \exp \left[-\frac{m_e^B \phi}{k_B T} \right] \approx \bar{n} \left[1 - \frac{m_e^B \phi}{k_B T} \right] \tag{31}$$

which leads to the following linearized Poisson-Boltzmann equation

$$\nabla^2 \phi = -4\pi G \bar{n} m_e^B + \frac{\phi}{\lambda_G^2} + GM\delta(r) \tag{32}$$

where the “halo” gravitational Debye length, λ_G , is expected to lie between the interstellar and intergalactic limits, although nearer the later limit, namely, $\lambda_G^s \ll \lambda_G \leq \lambda_G^g$. Equation (32) has solution

$$\phi(r) = \frac{k_B T}{m_e^B} - \frac{GM}{r} e^{-r/\lambda_G} \tag{33}$$

The gravitational potential energy for a mass m_e^B at distance r from the galactic center is, therefore,

$$\psi_e^B(r) = m_e^B \phi(r) = k_B T - \frac{GM m_e^B}{r} e^{-r/\lambda_G} \tag{34}$$

which consists of a thermal “off-set” term and a screened gravitational potential energy. The screening arises from the presence of other m_e^B masses which surround the central mass M .

From Eqs. (31) and (33) the electron Born mass density distribution is, therefore,

$$\begin{aligned} \mu_e^B(r) &= \bar{n} m_e^B \left[1 - \frac{m_e^B \phi(r)}{k_B T} \right] \\ &= \frac{1}{4\pi r \lambda_G^2} e^{-r/\lambda_G}. \end{aligned} \tag{35}$$

The rotational velocity of a star about the galactic center, at radius r , is given by

$$V = \sqrt{\frac{GM_{Tot}(r)}{r}} \quad (36)$$

where $M_{Tot}(r)$ is the total mass within radius r . In our later comparison with GRC galactic data we will already have including mass contributions from both the galactic bulge and disk, thus, we will only need to include contributions from DM in $M_{Tot}(r)$. Therefore

$$\begin{aligned} M_{Tot}(r) &= \int \mu_e^B(r) 4\pi r^2 dr \\ &= M_{eBDM} \left[1 - \left(1 + \frac{r}{\lambda_G} \right) \exp\left(-\frac{r}{\lambda_G}\right) \right], \end{aligned} \quad (37)$$

where M_{eBDM} is the total DM mass that surrounds the galaxy. From Eqs. (36) and (37) the rotational velocity that arises from eBDM can therefore be written as

$$V_{eBDM} = \sqrt{GM_{eBDM}/\lambda_G} f(x) \quad (38)$$

where the universal function

$$f(x) = \sqrt{\frac{1 - (1+x)\exp(-x)}{x}} \quad (39)$$

with the dimensionless variable $x = r/\lambda_G$. The function $f(x)$, which is plotted in Fig. 2, is universal because its shape is independent of the particular value of λ_G . The decay length, λ_G , is a rescaling of the r axis (assuming constant λ_G) while both M_{eBDM} and λ_G influence the magnitude of the DM rotational velocity according to Eq. (38).

Milky Way and M31 GRC analysis

Spiral galaxies typically consist of a central spherical bulge, of bulge radius $R_b \sim 2kpc$, upon which is superimposed a thin circular disk, of disk radius $R_d \sim 10kpc$ and disk thickness $T_d \sim 0.3kpc$. The bulge and disk, which are composed of dispersed stars, gas, and dust, are surrounded by a much larger and approximately spherical DM halo, of typical radius $R_h \sim 100kpc$. Stellar rotational velocities, about the galactic center, remain remarkable constant with velocities $V \sim 200km/s$, for galactic distances in the range $R \sim 1 - 20kpc$. Only at very large distances, $R \geq 40kpc$, do the rotational velocities decrease appreciably³¹.

The Sofue GRC data³¹ (gray data points, with Standard Deviation errors) for the Milky Way and M31 galaxies are shown in Figs. 3 and 4, respectively. This GRC data is an amalgamation of stellar rotational velocities along with satellite galaxy and global cluster velocities around the respective galactic centers. As a test of the reliability of the Sofue MW GRC data the Yu et al.³² binned MW data is also shown on Fig. 3 (red data points). The Yu binned MW data represents the analysis of 2,706 measurements of gas tracers, star tracers, and masers that have been arranged into 52 radial bins with approximately 52 measurements in each bin. As can be seen from Fig. 3 the Sofue GRC data is very similar to the Yu binned data, except that the Sofue data is systematically shifted upwards by approximately $18km/s$. This upward shift arises from differences in the assumed solar rotational velocity used as a calibration. Sofue assumes a solar rotational velocity of $V_0 = 238km/s$ at the Sun's radial distance from

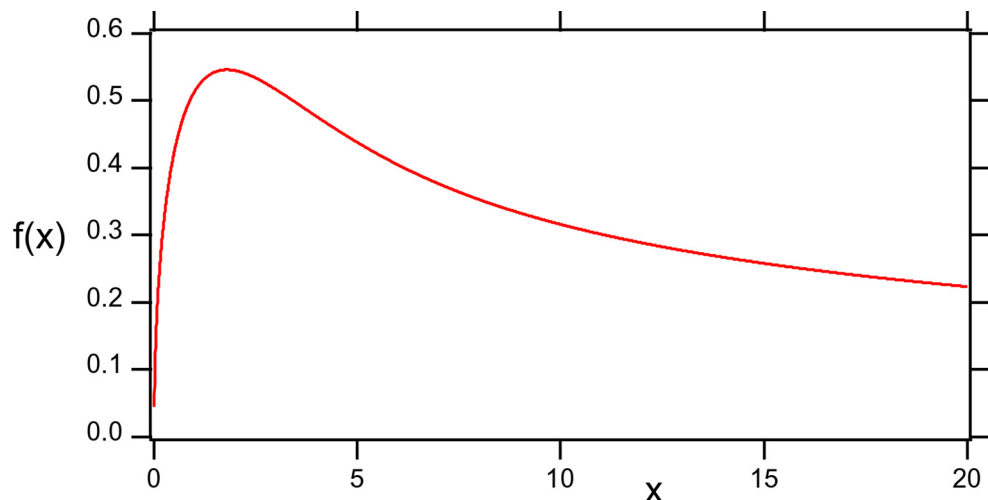


Figure 2. The universal function $f(x)$, Eq. (39), as a function of the dimensionless variable x .

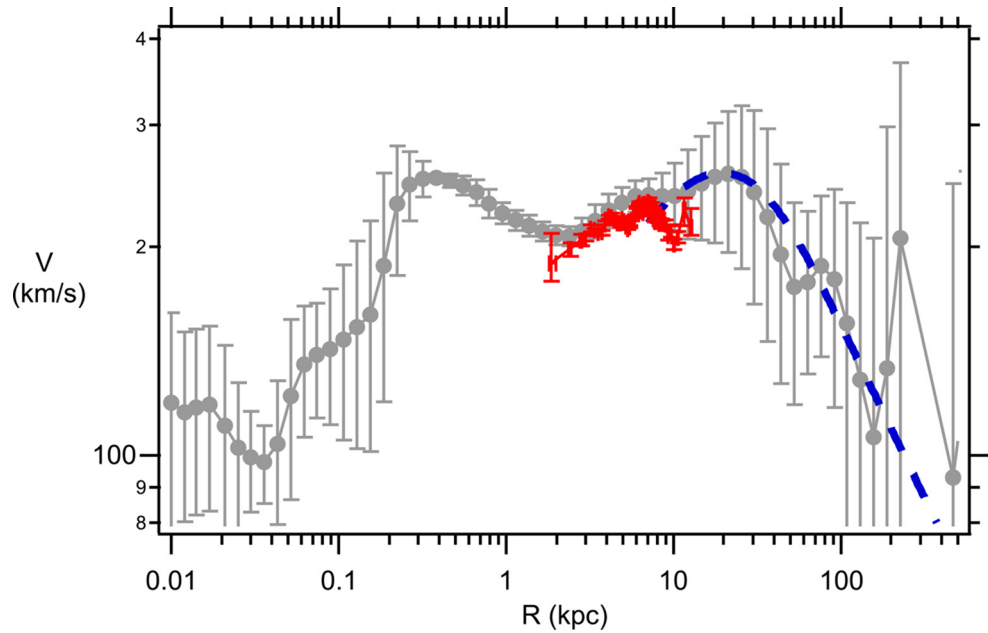


Figure 3. Milky Way GRC data from³¹ (gray data points including standard deviation errors). Data fit at large R using the eBDM model, Eqs. (38) and (39), with $\lambda_G = (10.9 \pm 1.2)kpc$ and $M_{eBDM} = (5.4 \pm 0.6) \times 10^{11}M_\odot$ (blue dashed line). Yu et al.³² data (red data points).

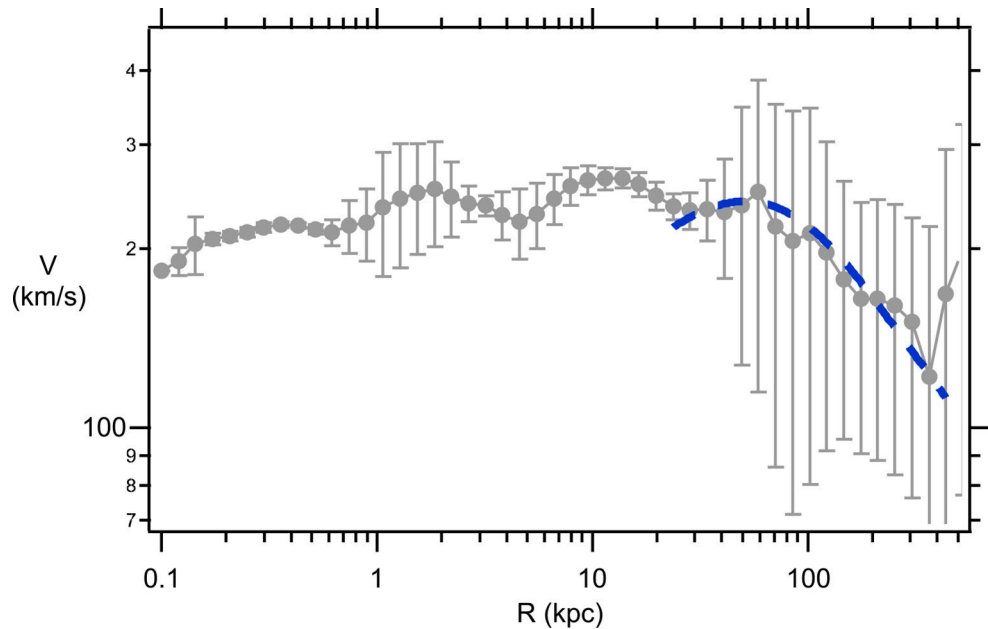


Figure 4. M31 GRC data from³¹ (gray data points including standard deviation errors). Data fit at large R using the eBDM model, Eqs. (38) and (39), with $\lambda_G = (28.6 \pm 2.6)kpc$ and $M_{eBDM} = (12.5 \pm 1.0) \times 10^{11}M_\odot$ (blue dashed line).

the galactic center of $R_0 = 8.0kpc$, whereas, Yu assumes a value of $V_0 = 220km/s$ at the same radial distance. The Sofue GRC data extends over a much, much larger range in R and, thus, is the most useful data set for ascertaining properties of the DM halo. Henceforth, any rotational velocities mentioned in this publication will be referring to the Sofue GRC data. For the MW (Fig. 3), the rotational velocities are approximately constant at $V \sim 230km/s$ for galactic distances in the range $R \sim 0.3 - 40kpc$. Rotational velocities are observed to drop precipitously for R in the range $\sim 40 - 400kpc$. A similar behavior is observed for the M31 galaxy (Fig. 4). In this case rotational velocities are approximately constant at $V \sim 230km/s$ for galactic distances in the range $R \sim 0.1 - 60kpc$. For $R \geq 60kpc$ there is a precipitous drop in V out to $R \approx 400kpc$. The influence of the DM

halo is expected to play the greatest role at large R , therefore, as a preliminary test of the suitability for using the eBDM model to describe DM Eqs. (38) and (39) were fitted to the mean MW and M31 GRC data, at large R . The blue dashed lines, in Figs. 3 and 4, show the best fit where the values for the best fit parameters, λ_G and M_{eBDM} , are listed in the figure captions. These preliminary comparisons indicate that the eBDM model may serve as a suitable model to describe DM.

Modeling galactic rotational velocities

In modeling galactic rotational velocities the usual assumption is that the composite rotational velocity $V(R)$ is composed of three velocity contributions arising from the galactic bulge $V_b(R)$, galactic disk $V_d(R)$, and DM halo $V_{DM}(R)$ where³¹

$$V(R)^2 = V_b(R)^2 + V_d(R)^2 + V_{DM}(R)^2 \quad (40)$$

and R is the galacto-centric distance.

The bulge contribution is frequently modeled using the de Vaucouleurs profile where the surface mass density³³

$$\Sigma_b(r) = \Sigma_{b0} \exp[-\kappa\{(r/R_b)^{1/4} - 1\}] \quad (41)$$

with $\kappa = 7.6695$ and Σ_{b0} is the surface mass density at the half mass scale radius $R = R_b$. The total bulge mass is then

$$M_b = 2\pi \int_0^\infty r \Sigma_b(r) dr = \eta R_b^2 \Sigma_{b0} \quad (42)$$

where $\eta = 22.665$. The bulge contribution to the rotational velocity is given by

$$V_b(R) = \sqrt{GM_b/R_b} B(X), \quad (43)$$

where

$$B(X) = \left[-\frac{4}{M_b X} \int_{r=0}^R r^2 \int_{x=r}^\infty \frac{d\Sigma_b(x)}{dx} \frac{1}{\sqrt{x^2 - r^2}} dx dr \right]^{1/2} \quad (44)$$

and $X = R/R_b$. It is readily shown, via a few changes of variables, that Eq. (44) is mathematically equivalent to

$$B(X) = \left[\frac{\kappa}{\eta X} \int_{Z=0}^X \int_{Y=1}^\infty \frac{Z^{5/4} \exp[-\kappa\{(ZY)^{1/4} - 1\}]}{Y^{3/4} \sqrt{Y^2 - 1}} dY dZ \right]^{1/2} \quad (45)$$

We experienced difficulties calculating $B(X)$, in the form given in Eq. (44), using Mathematica 13.3.1.0. Therefore, in these calculations, $B(X)$ was calculated using Eq. (45). Our $B(X)$ agrees well with the function given in Fig. 3 of³⁴, at both small and large X , however, there are differences near the peak of $B(X)$, which we attribute to differences in the numerical code used for calculating $B(X)$. A derivation of Eqs. (43)–(45), along with a graph of $B(X)$ (Fig. S1), is provided in the Supplementary Information.

The galactic disk is usually modeled using a thin exponential disk which gives rise to a rotation velocity given by³⁴

$$V_d(R) = \sqrt{GM_d/R_d} D(X), \quad (46)$$

where

$$D(X) = \frac{X}{\sqrt{2}} \left[I_0\left(\frac{X}{2}\right) K_0\left(\frac{X}{2}\right) - I_1\left(\frac{X}{2}\right) K_1\left(\frac{X}{2}\right) \right]^{1/2}, \quad (47)$$

$X = R/R_d$, R_d is the scale radius, M_d is the total mass within the disk, and I_i and K_i are modified Bessel functions.

In the Λ CDM model, the DM halo is frequently modeled using the NFW density profile³⁵ which is given by³⁴

$$\rho(r) = \rho_o/[Y(1+Y)^2], \quad (48)$$

where $Y = R/h$, and ρ_o and h are the representative density and scale radius, respectively. The enclosed mass, within radius R , is then

$$M_{NFW}(R) = 4\pi\rho_o h^3 [\ln(1+Y) - Y/(1+Y)] \quad (49)$$

which gives a rotation velocity of

Trial	R_b (kpc)	M_b ($10^{11}M_\odot$)	R_d (kpc)	M_d ($10^{11}M_\odot$)	h (kpc)	ρ_0 ($(10 \text{ pc})^{-3}M_\odot$)	χ^2
1 (Sofue)	0.87	0.25	5.73	1.12	10.7	18.2	8679
2	0.68 ± 0.09	0.18 ± 0.02					4946
3			6.9 ± 0.4	1.4 ± 0.1			3882
4					9.6 ± 1.0	22 ± 5	3757
5	0.70 ± 0.08	0.19 ± 0.02					3748
6			7.3 ± 0.4	1.5 ± 0.1			3637
7					9.0 ± 0.9	26 ± 6	3595
8	0.72 ± 0.08	0.19 ± 0.02					3589
9			7.6 ± 0.4	1.5 ± 0.1			3553
10					8.6 ± 0.9	28 ± 6	3534
11	0.71 ± 0.22	0.19 ± 0.05	8.2 ± 1.1	1.6 ± 0.3	7.4 ± 3.0	40 ± 41	3483
12 (SD)	0.54 ± 0.24	0.16 ± 0.06	5.2 ± 1.7	1.1 ± 0.9	15 ± 31	10 ± 47	3.3

Table 2. Λ CDM fit to Milky Way.

Trial	R_b (kpc)	M_b ($10^{11}M_\odot$)	R_d (kpc)	M_d ($10^{11}M_\odot$)	(kpc)	(M_\odot)	χ^2
1 (initial)	1	1	5	1	40	2	
2	0.96 ± 0.15	0.25 ± 0.03	6.91 ± 0.74	1.9 ± 0.4	31 ± 10	4.07 ± 0.55	3795
3 (SD)	0.55 ± 0.15	0.17 ± 0.04	4.7 ± 1.6	1.0 ± 1.0	20 ± 21	4.7 ± 2.4	3.1

Table 3. eBDM fit to Milky Way.

$$V_{NFW}(R) = \sqrt{GM_{NFW}(R)/R} \quad (50)$$

It should be noted that the NFW profile was not derived from any fundamental principles (i.e. it was not derived from the gravitational Poisson equation Eq. (25)). Instead the NFW profile arises from a guess for the best fit to gravitational simulation data for the galactic formation of DM halos.

In the chi-squared fitting procedure³⁶, used herein, a model for the composite rotational velocity V is fitted to the GRC data, V_i , by minimizing

$$\chi^2 = \sum_{i=1}^N \left(\frac{V - V_i}{w_i} \right)^2, \quad (51)$$

where w_i is the weight for each V_i , and N is the total number of data points. The minimization occurs by adjusting various parameters, within the function V , until χ^2 is a minimum. If V is a good representation of the data V_i , such that V_i is normally distributed about V (i.e. a Gaussian process), then upon taking w_i as the standard deviation σ_i then the expectation value for chi-squared should be³⁶

$$\langle \chi^2 \rangle = \nu = N - N_c, \quad (52)$$

where ν is the number of degrees of freedom, which is the difference between the number of data points N and the number of constraints N_c (i.e. the number of parameters that are actually adjusted to obtain the best fit).

In the Λ CDM model, the GRC data is chi-squared least-squares fitted using Eqs. (40), (43), (46), and (50) with 6 adjustable parameters, M_b and R_b for the bulge, M_d and R_d for the disk, and ρ_0 and h for the DM halo using the NFW profile. In the eBDM model, the NFW profile for DM, is replaced by Eqs. (38) and (39). In fitting the GRC data the 6 adjustable parameters are now, M_b and R_b for the bulge, M_d and R_d for the disk, and M_{eBDM} and λ_G for the DM halo.

For the Milky Way, the de Vaucouleurs profile does not fit the bulge at small R ³⁷, therefore, only GRC data in the range $0.2 \text{ kpc} \leq R \leq 500 \text{ kpc}$ is fitted. Additionally, the anomalous MW datum point, at $R \approx 226 \text{ kpc}$, has been excluded from all fits. The total number of data points fitted is $N = 39$. Tables 2 and 3 provide Λ CDM and eBDM fitting data to the Milky Way GRC data, respectively, while various fitting curves along with GRC data is provided in Fig. 5. As discussed earlier (and in the [Supplementary Information](#)) discrepancies in the calculation of $B(X)$ imply that the Sofue best fit values (Table 2, Trial 1) do not provide a good fit to the GRC data in the current calculation. Following the recommendation of Sofue³⁴ only the mean GRC data is fitted in the χ^2 fit (i.e. $w_i = 1$). The Standard Deviation (SD) errors are excluded from the fit, as including these errors would de-emphasize data at large R . (The issue of the SD errors will be examined later in this discussion.) In Table 2, to obtain the best fit to the GRC mean values, we sequentially cycle through fitting the bulge, and then the disk, and then the NFW halo. In any particular trial only 2 parameters are free to be adjusted for the best fit; the

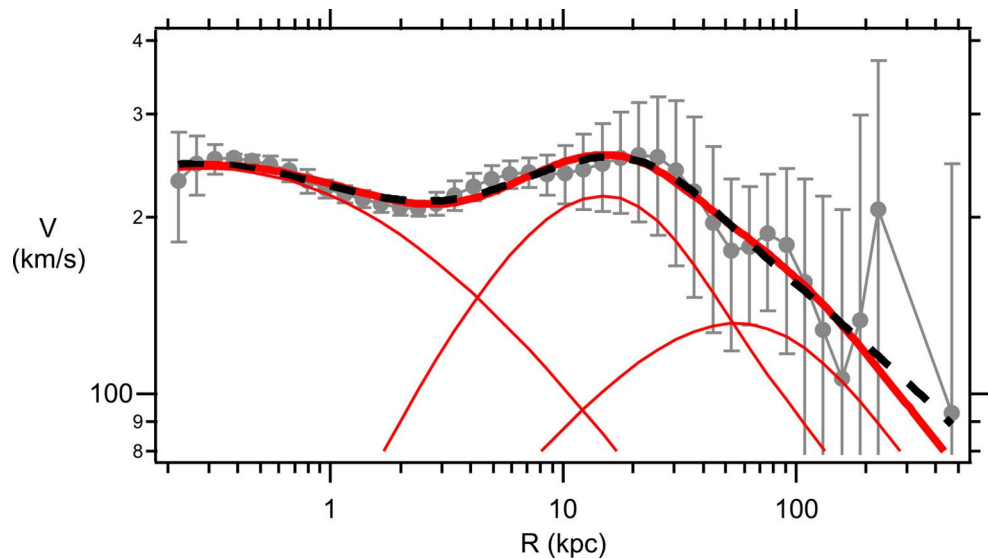


Figure 5. Milky Way GRC data (gray points with standard deviation errors). Best fit curve for Λ CDM Table 2 Trial 11 (black dashed line), eBDM Table 3 Trial 2 (red solid line). Three (lower) red solid curves, from left to right, V_b , V_d , and V_{eBDM} , which combine to eBDM Table 3 Trial 2. The anomalous datum point, at $R \approx 226$ kpc, has been excluded from all fits.

other 4 parameters are left fixed at their most recent best fit values. For example, in Table 2 Trial 5, the following 4 parameters were left **fixed** at their most recent best fit values of $R_d = 6.9$, $M_d = 1.4$, $h = 9.6$, $\rho_o = 22$, while the 2 parameters R_b and M_b were allowed to vary to find the lowest $\chi^2 (= 3748)$ value which resulted in $R_b = (0.70 \pm 0.08)$ kpc and $M_b = (0.19 \pm 0.02) \times 10^{11} M_\odot$. As one cycles through these various fits from Trial 1 to Trial 10 the χ^2 value steadily dropped from $\chi^2 = 8679$ down to $\chi^2 = 3534$, as the fit improves. One would hope that after 10 trials one would be close to the best fit minimum, corresponding to the lowest χ^2 . However, by cycling through in the manner described one is, by construction, constraining (or forcing) the model to fit the data. As a test to see if Trial 10 is indeed located near the lowest χ^2 all 6 parameters were allowed to vary in Trial 11 (where the best fit values, in Trial 10, were used as the initial values in Trial 11). A disturbing feature of Trial 11 is that ρ_o ballooned to $\rho_o = (40 \pm 41) \times (10 \text{ pc})^{-3} M_\odot$ where the error bar in ρ_o is larger than its mean value. This issue could be indicative that the NFW profile is not a good description of the GRC MW data. The Igor Pro 9.0.5.1 χ^2 fitting procedure, used in this calculation, uses the Levenberg-Marquardt algorithm which assumes that the fitting function is a good description of the data and that the errors are normally distributed. The estimated error, for each fitting coefficient, is determined from the residuals.

This χ^2 fitting issue, found for the Λ CDM fit, does not arise for the eBDM fit to the MW GRC data (Table 3). In this case, all 6 parameters were allowed to vary where the initial starting values are given in Table 3 Trial 1 and the resulting best fit values are given in Trial 2 of this table. In Table 3 Trial 2 all 6 error bars are less than their mean values, indicating that the eBDM model provides a good description of the data. Various best fit curves to the MW GRC data are shown in Fig. 5. Individual curves for V_b , V_d , and V_{eBDM} from Table 3 Trial 2 are shown in Fig. 5 (red solid lines), which provides a sense for the range in R over which the bulge, disk, and eBDM contribute the most to the composite rotational velocity V . The disk-DM radius, $R_{d/DM}$, defined by

$$V_d(R_{d/DM}) = V_{DM}(R_{d/DM}) \quad (53)$$

determines whether galactic disk matter or DM dominates the composite rotation velocity. When $R > R_{d/DM}$ ($< R_{d/DM}$) DM (galactic disk material) dominates the composite rotational velocity V . From Fig. 5 $R_{d/eBDM}(MW) = 53 \text{ kpc}$ for the eBDM model. DM is expected to be the dominant constituent of most galaxies. In the eBDM model, for the Milky Way, the percentage of DM is given by

$$DM_{eBDM}(MW) = \frac{M_{eBDM}}{M_b + M_d + M_{eBDM}} \times 100\% = 65\% \quad (54)$$

which indeed indicates that the MW is dominated by DM, as expected. One can draw a number of interesting conclusions from Fig. 5, for the eBDM model. The individual V_b , V_d , and V_{eBDM} curves, in this model, indicate that the observed flat rotation curve in the range $0.3 \text{ kpc} < R < 20 \text{ kpc}$, for the MW, arises primarily from the distribution of matter in the galactic bulge and galactic disk. DM only becomes the dominant component for $R > R_{d/eBDM}(MW) = 53 \text{ kpc}$ and, hence, plays a minor role in flattening the MW GRC curve (at $0.3 \text{ kpc} < R < 20 \text{ kpc}$).

The MW is known to exhibit prominent dips in the rotational velocities at radii of $\sim 3 \text{ kpc}$ and $\sim 9 \text{ kpc}$ ³³. These rotational dips are thought to arise from internal structure within the galactic disk. The model considered

Trial	R_b (kpc)	M_b ($10^{11} M_\odot$)	R_d (kpc)	M_d ($10^{11} M_\odot$)	h (kpc)	ρ_o ($(10 \text{ pc})^{-3} M_\odot$)	χ^2
1(Sofue)	1.35	0.35	5.28	1.26	34.6	2.23	15782
2	1.8 ± 0.2	0.39 ± 0.04					7527
3			5.8 ± 0.4	1.3 ± 0.1			7112
4					29 ± 3	3.0 ± 0.8	7665
5	1.9 ± 0.2	0.40 ± 0.04					6642
6			5.8 ± 0.4	1.2 ± 0.1			6512
7					26 ± 3	4.1 ± 0.9	6350
8	1.9 ± 0.2	0.41 ± 0.04					6232
9			5.9 ± 0.5	1.1 ± 0.1			5962
10					25 ± 3	4.8 ± 1.0	5850
11	2.0 ± 0.2	0.43 ± 0.04					5818
12			6.0 ± 0.5	1.08 ± 0.11			5629
13					23 ± 2	5.3 ± 1.1	5552
14	2.1 ± 0.2	0.45 ± 0.04					5520
15			6.1 ± 0.5	1.0 ± 0.1			5405
16					23 ± 2	5.8 ± 1.1	5347
17	1.95 ± 0.43	0.40 ± 0.11	5.1 ± 2.5	0.24 ± 0.42	13 ± 5	25 ± 22	4436
18 (SD)	1.25 ± 0.23	0.25 ± 0.05	4.2 ± 0.9	0.7 ± 0.6	17 ± 17	12 ± 26	6.8

Table 4. Λ CDM fit to M31.

Trial	R_b (kpc)	M_b ($10^{11} M_\odot$)	R_d (kpc)	M_d ($10^{11} M_\odot$)	(kpc)	(M_\odot)	χ^2
1 (initial)	1	1	5	1	40	2	
2	2.4 ± 0.3	0.53 ± 0.08	5.6 ± 0.8	1.0 ± 0.2	38 ± 4	11.4 ± 0.7	4015
3 (SD)	1.4 ± 0.2	0.28 ± 0.05	4.5 ± 0.7	1.2 ± 0.3	40 ± 17	12 ± 6	6.9

Table 5. eBDM fit to M31.

in this publication is axisymmetric, namely, the model only depends upon the galactic distance, R , and there is no angular dependence within the galactic disk. An axisymmetric exponential disk model, therefore, only captures the average physical features of galactic spiral arms and will be incapable of describing these rotational dips. Sofue, Honma, and Omodaka³³ have examined what type of internal features, within the spiral arms, may be the cause for the rotational dips observed in the MW GRC data.

This same χ^2 fitting scheme is applied to the M31 GRC data in Tables 4 and 5, and Fig. 6 for data in the range $0.1 \text{ kpc} \leq R \leq 400 \text{ kpc}$. The number of data points is $N = 46$, in this case. After 16 trials (Table 4) one would hope that the lowest χ^2 had been determined for the Λ CDM model, however, upon allowing all 6 parameters to vary (Table 4, Trial 17) both M_d and ρ_o are found to have ballooned to $M_d = (0.24 \pm 0.42) \times 10^{11} M_\odot$ and $\rho_o = (25 \pm 22) \times (10 \text{ pc})^{-3} M_\odot$, in a similar manner to what was found for the MW GRC data. By contrast with this problematic Λ CDM behavior, the eBDM fit does not experience the same difficulties, and the best fitting parameters are readily fit without any of the parameters ballooning out of control (Table 5 Trial 2). Various best fit curves to the M31 GRC data are shown in Fig. 6. Individual curves for V_b , V_d , and V_{eBDM} from Table 5 Trial 2 are shown in Fig. 6 (red solid lines), which provides a sense of the range in R over which the bulge, disk, and eBDM contribute the most to the composite rotational velocity V . The Dark Matter content for M31 is, in this case, $DM_{eBDM}(M31) = 88\%$ where $R_{d/eBDM}(M31) = 20 \text{ kpc}$. In the eBDM model the flat rotation curve for M31, which extends from $R \sim 0.2 \text{ kpc}$ through to $R \sim 70 \text{ kpc}$ (Fig. 6), is primarily dominated by the luminous galactic bulge and disk material for $R < R_{d/eBDM}(M31) = 20 \text{ kpc}$ and DM only significantly contributes to flattening the rotation curves at $R > R_{d/eBDM}(M31) = 20 \text{ kpc}$.

The influence of the large SD errors, σ_i , upon the χ^2 fitting procedure is examined by setting the weight $w_i = \sigma_i$. For this fit, there is much more “parameter space” within which each fitting parameter can vary. Table 2 Trial 12 shows the results for the Λ CDM fit to the MW GRC data where, in this fitting procedure, the Trial 10 results were used as the initial values. $M_d = 1.1 \pm 0.9$, $h = 15 \pm 31$, and $\rho_o = 10 \pm 47$ have ballooned out of control. For the eBDM fit to the MW GRC data (Table 3 Trial 3) both $M_d = 1.0 \pm 1.0$ and $\lambda_G = 20 \pm 21$ have ballooned out of control. The ballooning is much worse for the Λ CDM model than for the eBDM model. Both fits have $\chi^2 \sim 3$, which is much less than the expectation value of $\langle \chi^2 \rangle = N - N_c = 39 - 6 = 33$. This low χ^2 value is indicative that the SD errors are non-Gaussian and too large. Yu et al.³² also have found, in a separate analysis of MW data, that the SD errors were non-Gaussian.

The SD χ^2 fit to the M31 GRC data is given in Table 4 Trial 18 and Table 5 Trial 3 for, respectively, the Λ CDM and eBDM models. As was found for the MW GRC data, the eBDM model fits the M31 GRC data better than the Λ CDM model. The $\chi^2 \sim 6.9$ is much lower than the expectation value of $\langle \chi^2 \rangle = N - N_c = 45 - 6 = 39$

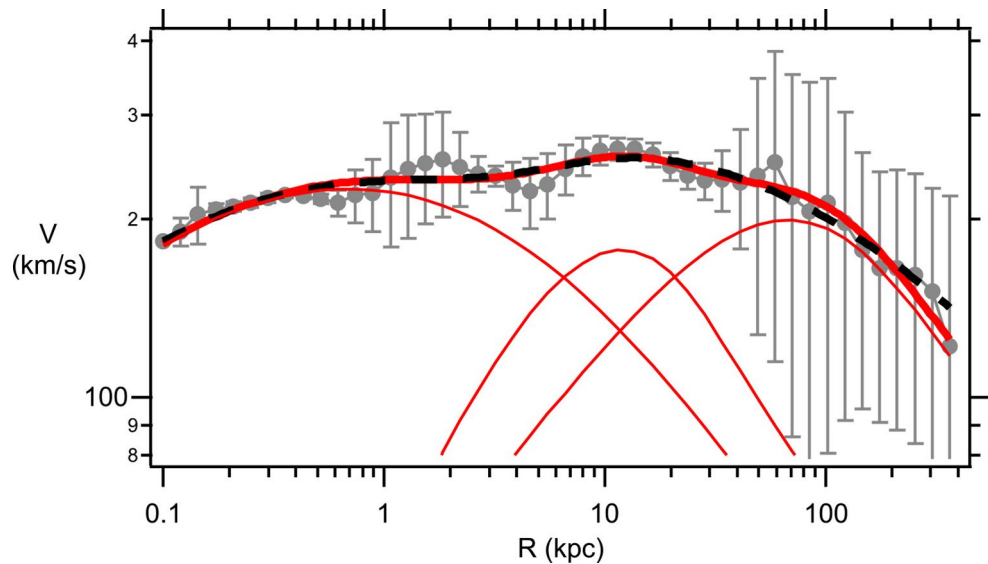


Figure 6. M31 GRC data (gray points with standard deviation errors). Best fit curve for Λ CDM Table 4 Trial 17 (black dashed line), eBDM Table 5 Trial 2 (red solid line). Three (lower) red solid curves, from left to right, V_b , V_d , and V_{eBDM} , which combine to eBDM Table 5 Trial 2.

indicating again that the SD errors are non-Gaussian and too large. (Note that in this fit $N = 45$ because one datum point at $R_i = 0.1 \text{ kpc}$ did not have a SD and, therefore, was omitted from the fitting procedure.)

Summary and discussion

Any theory for DM must derive from the gravitational Poisson equation (Eq. (25)). If DM is a *particle* then this particle must obey the still more restrictive linearized Poisson-Boltzmann (IPB) equation. For a DM particle possessing an attractive gravitational interaction the IPB takes the form given in Eq. (28) and any galactic halo, formed from such particles, would be subjected to a gravitational instability and one would need to consider whether or not such a DM halo could remain stable over time periods of billions of years. By contrast, if the DM particle possesses a repulsive gravitational interaction the IPB takes the form given in Eq. (32) which would ensure the stability of the DM halo against gravitational collapse. Any theory for DM must also be able to explain the typical DM halo size, of order $\sim 100 \text{ kpc}$, as well as, provide a quantitative description of GRC data for the rotational velocities of stars, satellite galaxies, and globular clusters about the galactic center.

In this publication earlier work on the eBse model^{15–17} is extended to the DM galactic halo. The resultant eBDM profile possesses a repulsive gravitational interaction where the IPB gives rise to the DM rotational velocity V_{eBDM} in Eqs. (38)–(39). Upon combining the de Vaucouleurs profile (Eqs. (43) and (45)) for the galactic bulge, and the exponential profile (Eqs. (46) and (47)) for the galactic disk, with the eBDM profile for the galactic DM halo, the resultant velocity (Eq. (40)) provides a good description of the GRC data for both the Milky Way (Table 3 and Fig. 5) and M31 (Table 5 and Fig. 6) galaxies. In comparison, the Λ CDM model, where the NFW profile (Eqs. (49)–(50)) is used to describe the DM halo (in place of the eBDM profile), the NFW profile does not describe the GRC data as well for both the Milky Way and M31 galaxies -- see Table 2, Trial 11 and Table 4, Trial 17 and the resultant discussion.

The eBDM model additionally provides natural explanations for a number of features associated with DM:

- (i) The Born mass, m_e^B , is a feature of free electrons in the eBse model and will be present at all length scales and, hence, will influence galactic, as well as, cosmological astrophysical phenomena. m_e^B only interacts gravitationally, and cannot be detected via any other means, which would explain why DM has not been detected directly thus far.
- (ii) In the eBDM model the typical size of a DM galactic halo is expected to be of order the intergalactic gravitational Debye length $\lambda_G^g \approx 91 \text{ kpc}$ (Table 1).
- (iii) In the Λ CDM model baryons and DM are expected to be uncorrelated, however, there is documented evidence (e.g. the Tully-Fisher relationship³⁸) that there is a tight correlation between DM and baryons in galaxies. As the number of free electrons, in a galaxy, should be related to the number of baryons this suggests that, in the eBse model, there will be a tight correlation between eBDM and baryons in this model. An examination of this issue will be left to future research.
- (iv) In the NFW profile, used in the Λ CDM model, there is a “cuspy halo” problem at small R ^{13,39}, namely, the DM density diverges as $\rho(R) \sim 1/R$ at small R (Eq. (48)). In reality DM is thought to be “flat”, rather than divergent, as $R \rightarrow 0$. In the eBDM model, at large $R \sim R_h \sim 100 \text{ kpc}$, the gravitational Debye length λ_G is expected to be of order $\lambda_G^g \approx 91 \text{ kpc}$. However, at small R , of order the bulge radius $R_b \sim 2 \text{ kpc}$, λ_G is expected to cross-over to the interstellar gravitational Debye length $\lambda_G^s \approx 0.009 \text{ kpc}$. For very, very small $R \ll R_b$ the physics will be controlled by the Coulomb interaction, between charged particles, rather

than any gravitational interaction. Hence, in the limit $R \rightarrow 0$ we do not expect there to be a divergence in the DM density in the eBDM model. Note also, from Eq. (37), $M_{Tot}(R=0) = 0$, in other words, in the eBDM model there is no divergent DM mass contribution at the origin.

- (v) In the CDM scenario, there is a “missing satellites” problem where too many satellite galaxies are predicted to be orbiting the galactic center of large galaxies^{40,41}. The eBDM model, along with associated baryon content, would need to be incorporated within galactic simulations before it is known what the eBDM model predicts.
- (vi) DM is expected to induce structure formation where baryonic matter falls into the potential wells created by DM particles. The first line in Eq. (30) is valid in general, for any situation, where M represents a point mass at the origin. In the Section “Rotational velocities around a galactic center” we considered the situation where M was of order the galactic mass in order to derive the eBDM rotational velocity $V_{eBDM}(R)$ (Eqs. (38) and (39)). Alternatively, for a gaseous medium ($\mu = 0$) and with $M = m_e^B$, Eq. (30) (when combined with the continuity and Euler equations) would describe both the repulsion between neighboring Born masses, as well as, the gravitational collapse of gaseous hydrogen, helium, and protons into the deep potential well created by each eBDM particle, due to the large Born mass ($m_e^B \approx 40m_p$, Eq. (11)).
- (vii) The astronomical literature is replete with claims that “flat rotation curves provide evidence for DM”. The current analysis indicates that such claims should be treated with caution, especially if the claims are based upon rotational velocities that only extend out to galactic radii of $R \sim 10 - 20kpc$ (i.e. typical stellar rotational velocities). Figures 5 and 6 indicate that flat rotation curves out to $R \sim 10 - 20kpc$, for the Milky Way and M31 galaxies, are primarily determined by the mass distribution of baryonic matter in the galactic bulge and galactic disk. Only at much larger radii, $R > R_{d/DM}$ (Eq. (53)), does DM play a significant role in determining the rotational velocities around galactic centers. $R_{d/eBDM}(MW) = 53kpc$ while $R_{d/eBDM}(M31) = 20kpc$, therefore, the best evidence for DM from composite rotational velocities V arises at very large $R \approx 30 - 400kpc$ where the standard deviation errors in V are also unfortunately large. Prior analysis³¹, where the NFW profile was used to model the DM halo, would also seem to support this conclusion.

To reiterate, in studying DM contributions from rotational velocities, it is very important to (a) accurately model the baryonic contributions from both the galactic bulge and galactic disk and (b) study rotational velocities at very large $R > R_{d/DM}$ where the DM contributions are greatest. Hence, studies of galactic Grand Rotation Curves (which include contributions from stars, satellite galaxies, and globular clusters) will provide more definitive information about DM than studies of galactic Rotation Curves (which only include contributions from stars). The close proximity of the Milky Way and M31 galaxies imply that their GRC data are likely to be very accurate and, hence, will serve as ideal candidates for the study of DM.

- (viii) A MOND-like theory, which incorporated a Yukawa potential⁴², has recently been able to describe the GRC data for the Milky Way and M31 galaxies. V_{eBDM} , Eqs. (38)–(39), is similar to their apparent DM velocity, which would explain why these authors were able to obtain a good description of the GRC data. The Yukawa length, λ_Y (where λ_Y replaces λ_G in Eq. (39)), that appears in such modified gravity theories is expected to be a **universal constant**^{43,44}. However, considerable variation in $\lambda_Y \sim 5 - 50kpc$ is observed from galaxy to galaxy^{43,44}, thus, λ_Y does not appear to be universal. (Note: these estimates for λ_Y were deduced by modeling the baryonic component using an exponential disk⁴³ (i.e. no galactic bulge) at small galactic distances of $R \sim 0 - 25kpc$, hence, breaking both rules (a) and (b) in comment (vii) above). The expectation of a universal Yukawa length λ_Y , in modified gravity theories, should be contrasted with the eBDM model where the gravitational Debye length, λ_G , is expected to vary from galaxy to galaxy, depending upon the value of T/\bar{n} in Eq. (24).

The eBse model is a “package deal”, namely, if this model is correct it is expected to describe DE^{15,16}, DM, as well as, CI¹⁷. The construction of the eBse model is such that it is not possible to accept part of the model (e.g. DE) and reject the other two components (CI and DM) as this would lead to internal inconsistencies within the eBse model. As there is significant observational evidence for DM, the success or failure of the eBse model is therefore likely to hinge upon how well eBDM continues to describe these DM observations.

Data availability

All data generated or analyzed during this study are included in this published article.

Received: 24 July 2024; Accepted: 30 September 2024

Published online: 15 October 2024

References

- Ostriker, J. P. & Steinhardt, P. New light on Dark Matter. *Science* **300**, 1909–1913 (2003).
- Bertone, G. & Hooper, D. History of dark matter. *Rev. Mod. Phys.* **90**, 045002 (2018).
- Ellis, R. S. Gravitational lensing: a unique probe of dark matter and dark energy. *Phil Trans. R Soc. A* **368**, 967–987 (2010).
- Courteau, S. et al. Galaxy masses. *Rev. Mod. Phys.* **86**, 47–119 (2014).
- Rubin, V. C. & Ford, W. K. Rotation of the andromeda nebula from a spectroscopic survey of emission regions. *Astrophys. J.* **159**, 379–403 (1970).
- Rubin, V. C., Ford, J. & Thonnard, N. Rotational properties of 31 sc galaxies with a large range of luminosities and radii, from NGC 4605 (R = 4 kpc) to UGC 2885 (R = 122 kpc). *Astrophys. J.* **238**, 471–487 (1980).
- Sofue, Y. & Rubin, V. Rotation curves of spiral galaxies. *Annu. Rev. Astron. Astrophys.* **39**, 137–174 (2001).
- Zwicky, F. On the masses of nebulae and of clusters of nebulae. *Astrophys. J.* **86**, 217–246 (1937).

9. Ostriker, J. P. & Peebles, P. J. E. A numerical study of the stability of flattened galaxies: or, can cold galaxies survive? *Astrophys. J.* **186**, 467–480 (1973).
10. Clowe, D., Gonzalez, A. & Markevich, M. Weak lensing mass reconstruction of the interacting cluster 1E0657-558: direct evidence for the existence of dark matter. *Astrophys. J.* **604**, 596–603 (2004).
11. Markevich, M. et al. Direct constraints on the dark matter self-interaction cross-section from the merging galaxy cluster 1E0657-56. *Astrophys. J.* **606**, 819–824 (2004).
12. PlanckCollaboration. Planck 2018 results. VI. Cosmological parameters. *Astron. Astrophys.* **641**, A6 (2020).
13. Clifton, T., Ferreira, P. G., Padilla, A. & Skordis, C. Modified gravity and cosmology. *Phys. Rep.* **513**, 1–189 (2012).
14. Milgrom, M. MOND vs. dark matter in light of historical parallels. *Stud. Hist. Philos. Mod. Phys.* **71**, 170–195 (2020).
15. Law, B. M. Cosmological consequences of a classical finite-sized electron model. *Astrophys. Space Sci.* **365**, 64 (2020).
16. Law, B. M. Electron Born self-energy model for Dark Energy. *Phys. Sci. Forum* **2**, 9 (2021).
17. Law, B. M. Proposed physical mechanism that gives rise to cosmic inflation. *Sci. Rep.* **13**, 21788 (2023).
18. Dodelson, S. & Schmidt, F. *Modern Cosmology* 2nd edn (Elsevier, 2021).
19. Spergel, D. N. et al. Three-year Wilkinson microwave anisotropy probe (WMAP) observations: implications for cosmology. *Astrophys. J. Supplement Ser.* **170**, 377–408 (2007).
20. Frieman, J. A., Turner, M. S. & Huterer, D. Dark Energy and the accelerating Universe. *Annu. Rev. Astron. Astrophys.* **46**, 385–432 (2008).
21. Farooq, O., Madiyar, F. R., Crandall, S. & Ratra, B. Hubble parameter measurement constraints on the redshift of the deceleration-acceleration transition, dynamical Dark Energy, and space curvature. *Astrophys. J.* **835**, 1–11 (2017).
22. Bourilkov, D. Hint for axial-vector contact interactions in the data on $e^+e^-e^+e^-(g)$ at center-of-mass energies 192–208 GeV. *Phys. Rev. D* **64**, 071701R (2001).
23. Gabrielse, G., Hanneke, D., Kinoshita, T., Nio, M. & Odom, B. New determination of the fine structure constant from the electron g value and QED. *Phys. Rev. Lett.* **97**, 030802 (2006).
24. Israelachvili, J. N. *Intermolecular and Surface Forces* 3rd edn (Academic, 2011).
25. Feynman, R. P., Leighton, R. & Sands, M. *The Feynman Lectures on Physics*. Vol. II Chaps. 8 & 28 (Addison-Wesley, 1964).
26. Cen, R. & Ostriker, J. P. Where are the baryons? II. Feedback effects. *Astrophys. J.* **650**, 560–572 (2006).
27. Sick, I. Nucleon radii. *Prog. Part. Nucl. Phys.* **55**, 440 (2005).
28. Thorne, K. S. & Blandford, R. D. *Modern Classical Physics* (Princeton University Press, 2017).
29. Landau, L. D. & Lifshitz, E. M. *The Classical Theory of Fields* (Pergamon, 1975).
30. Gorbunov, D. S. & Rubakov, V. A. *Introduction to the Theory of the Early Universe: Cosmological Perturbations and Inflationary Theory* (World Scientific Publishing Co., 2011).
31. Sofue, Y. Dark halos of M31 and the Milky Way. *Publ. Astron. Soc. Japan* **67**, 75 (2015).
32. Yu, H., Singal, A., Peyton, J., Crandall, S. & Ratra, B. Gaussian processes, median statistics, Milky Way rotation curves. *Astrophys. Space Sci.* **365**, 146 (2020).
33. Sofue, Y., Honma, M. & Omodaka, T. Unified rotation curve of the Galaxy - decomposition into de vaucouleurs bulge, disk, dark halo, and the 9-kpc rotation dip. *Publ. Astron. Soc. Japan* **61**, 227 (2009).
34. Sofue, Y. Grand rotation curve and dark-matter halo in the Milky Way galaxy. *Publ. Astron. Soc. Japan* **64**, 75 (2012).
35. Navarro, J. F., Frenk, C. S. & White, S. D. M. The structure of Cold Dark Matter halos. *Astrophys. J.* **462**, 563 (1996).
36. Bevington, P. R. & Robinson, D. K. *Data Reduction and Error Analysis* 3rd edn (McGraw-Hill, 2003).
37. Sofue, Y. Rotation curve and mass distribution in the galactic center - from black hole to entire galaxy. *Publ. Astron. Soc. Japan* **65**, 118 (2013).
38. McGaugh, S. S., Schombert, J. M., Bothun, G. D. & De Blok, W. The baryonic Tully-Fisher relation. *Astrophys. J.* **533**, L99–L102 (2000).
39. de Blok, W. The core-cusp problem. *Adv. Astronomy* **0910.3538**, 789293 (2010).
40. Mateo, M. L. Dwarf galaxies of the local group. *Ann. Rev. Astron. Astrophys.* **36**, 435–506 (1998).
41. Klypin, A., Kravtsov, A., Valenzuela, O. & Prada, F. Where are the missing galactic satellites?. *Astrophys. J.* **522**, 89–92 (1999).
42. D'Agostino, R., Jusufi, K. & Capozziello, S. Testing Yukawa cosmology at the Milky Way and M31 galactic scales. *Eur. Phys. J. C* **84**, 386 (2024).
43. Moffat, J. W. & Rahvar, S. The MOG weak field approximation and observational test of galaxy rotation curves. *MNRAS* **436**, 1439–1451 (2013).
44. Roshan, M. & Mashhoon, B. Characteristics of effective dark matter in nonlocal gravity. *Astrophys. J.* **934**, 9 (2022).

Acknowledgements

The author thanks Professor Yoshiaki Sofue for access to the Milky Way and M31 GRC data, as well as, to his publication resources. The author thanks Professor Bharat Ratra for useful comments.

Author contributions

The author is solely responsible for all calculations, conclusions, and statements in this publication.

Declarations

Competing interests

The authors declare no competing interests.

Additional information

Supplementary Information The online version contains supplementary material available at <https://doi.org/10.1038/s41598-024-74884-6>.

Correspondence and requests for materials should be addressed to B.M.L.

Reprints and permissions information is available at www.nature.com/reprints.

Publisher's note Springer Nature remains neutral with regard to jurisdictional claims in published maps and institutional affiliations.

Open Access This article is licensed under a Creative Commons Attribution 4.0 International License, which permits use, sharing, adaptation, distribution and reproduction in any medium or format, as long as you give appropriate credit to the original author(s) and the source, provide a link to the Creative Commons licence, and indicate if changes were made. The images or other third party material in this article are included in the article's Creative Commons licence, unless indicated otherwise in a credit line to the material. If material is not included in the article's Creative Commons licence and your intended use is not permitted by statutory regulation or exceeds the permitted use, you will need to obtain permission directly from the copyright holder. To view a copy of this licence, visit <http://creativecommons.org/licenses/by/4.0/>.

© The Author(s) 2024